Combined negative dielectrophoresis and phase separation in nondilute suspensions subject to a high-gradient ac electric field

Anil Kumar,* Zhiyong Qiu,† and Andreas Acrivos‡
The Levich Institute, The City College of New York, 140th Street & Convent Avenue, New York, New York 10031, USA

Boris Khusid§
New Jersey Institute of Technology, University Heights, Newark, New Jersey 07102, USA

David Jacqmin‖
NASA Glenn Research Center, Cleveland, Ohio 44135, USA

(Received 26 August 2003; published 24 February 2004)

Experiments were conducted on concentrated suspensions of neutrally buoyant particles which exhibit negative dielectrophoresis. We found that, due to interparticle electrical interactions, such suspensions undergo a phase separation when subjected to a high-gradient ac field ($\sim$kV/mm) and form a propagating distinct front between the regions enriched with and depleted of particles. A generalization of our theory for the thermodynamics of the field-induced phase transitions in suspensions of polarized particles [Phys. Rev. E **52**, 1669 (1995); **54**, 5428 (1996); **60**, 3015 (1999)] is proposed for the front propagation, and its predictions are shown to be consistent with the experiments even though the model contains no fitting parameters. The combination of field-induced dielectrophoresis and phase transition provides a method for strongly concentrating particles in prespecified regions of dielectrophoretic devices.

DOI: 10.1103/PhysRevE.69.021402 PACS number(s): 82.70.Kj, 85.50.−n, 77.84.Nh, 77.22.Gm

I. INTRODUCTION

When exposed to a spatially nonuniform electric field, a particle experiences a force which includes two terms. The first, being the product of the particle charge and the field strength, is known as the electrophoretic force. The other, being the product of the particle dipole moment and the gradient of the field strength, is referred to as the dielectrophoretic force [1]. Since the particle dipole moment is proportional to the field strength, the dielectrophoretic force appears to be proportional to the gradient of the square of the field strength. Electrophoretic effects vanish in an ac field of a sufficiently high frequency due to the zero time average of the electrophoretic force. In contrast, dielectrophoresis operates in high-frequency fields because the dielectrophoretic force averaged over the field oscillations gives a nonzero value. The past decade has seen a spectacular increase in the use of ac dielectrophoretic phenomena for trapping, concentrating, and sorting of colloidal particles, cells, microorganisms, and biomolecules [2–12]. The essential advantage of these techniques is that ac fields suppress undesirable electric effects in a liquid such as electrolysis and electroconvection that makes them particularly well suited for microfluidic applications [2,3]. The ac dielectrophoretic force acting on a sphere immersed in a liquid is [4]

$$\mathbf{F}_{\mathrm{dep}}=\frac{3}{2}\varepsilon_0\varepsilon_{\mathrm{f}}v_{\mathrm{p}}\,\mathrm{Re}[\beta(\omega)]\nabla\langle\mathbf{E}^2\rangle, \tag{1}$$

where v_{p} is the particle volume, ε_0 is the vacuum permittivity, ε_{f} is the dielectric constant of the liquid, $\mathrm{Re}(\beta)$ is the real part of the relative particle polarization β at the field frequency ω, and $\langle\ \rangle$ denotes time averaging over the field oscillation. Depending on the sign of $\mathrm{Re}(\beta)$, the particle moves toward the regions of high field strength (positive dielectrophoresis) or low field strength (negative dielectrophoresis). In our recently published papers [13,14], we demonstrated that the predictions of a single-particle model which only takes into account the dielectrophoretic force, Eq. (1), the Stokes drag force, and the gravity force acting on a particle are consistent with experimental data for dilute suspensions containing $\sim$0.1% (v/v) of positively and negatively polarized particles. Since the single-particle model ignores the interparticle electric and hydrodynamic interactions, it does not predict the appearance of field-induced particle aggregation in high-gradient ac fields which governs eventually the particle spatial arrangement. We also demonstrated [15] that the presence of the interparticle dipole-dipole interactions imposes a lower bound on the scale of microelectrode arrays for the precise positioning of positively polarized particles in selected locations of a dielectrophoretic microchannel even for dilute suspensions of $\sim$0.1% (v/v). In Ref. [16], we reported observations of a new phenomenon in dilute, $\sim$0.1% (v/v), suspensions of negatively polarized particles flowing through a microchannel in which they were subjected to a high-gradient ac field and shear. Specifically, these particles were found to undergo a phase transition and form a highly concentrated ''bolus'' when the applied field forced them to be confined at the entrance region of a dielectrophoretic gate. We also presented [16] the main features of our theory for the effects of the interparticle interactions on the field-induced phase transitions in suspension whose predictions for the bolus formation were qualitatively consistent with the experimental results.

*Electronic address: anil@levdec.engr.ccny.cuny.edu
†Electronic address: qiu@lisgi6.engr.ccny.cuny.edu
‡Electronic address: acrivos@scisun.sci.ccny.cuny.edu
§Electronic address: khusid@adm.njit.edu
‖Electronic address: fsdavid@tess.lerc.nasa.gov

The purpose of this article is to study quantitatively, both experimentally and theoretically, a field-induced phase transition in concentrated suspensions $\sim 5\%-15\%$ (v/v) of neutrally buoyant, negatively polarized particles under the action of a high-gradient ac electric field. Following the field application, such suspensions are found to undergo a phase separation and form a propagating distinct front between the regions enriched with and depleted of the particles. This phenomenon driven by the interparticle electric and hydrodynamic interactions constitutes a method for strongly concentrating particles in focused regions of dielectrophoretic devices.

The organization of the article is as follows. In Sec. II, we briefly describe the suspension properties and the experimental setup being used. A more detailed description of the experimental procedures can be found in Refs. [13,14]. In Sec. III, we present experimental data on the field-induced formation and propagation of the concentration front. In Sec. IV, we describe a theory for the electrohydrodynamics of a concentrated suspension subjected to a high-gradient ac field and shear the main features of which were only briefly outlined in Ref. [16] due to space limitations. The comparison of the theoretical predictions with the experimental data is given in Sec. V. The model calculations require no fitting parameters since the suspension characteristics were measured independently. In Sec. VI, we consider a mechanism for the experimentally observed accumulation of the particles in the region of high-field strength near the high-voltage electrodes where, according to Eq. (1), the particles should have been repelled. The main conclusions are summarized in Sec. VII.

II. EXPERIMENTAL PROCEDURES

A. Materials

The suspension consisted of neutrally buoyant spherical polyalphaolefin particles (AVEKA, Woodbury, MN) suspended in Mazola corn oil ($\rho_f = 0.92$ g/cm^3, $\eta_f = 59.7$ cp at 23 °C). The particle size distribution on a number basis was measured with a Beckman-Coulter laser diffraction particle size analyzer LS 230 and the average diameter of the particles was found to be 87 μm with 80% of them having diameters between 68 and 116 μm. The dielectric permittivities of the suspension, ε_s^*, and that of the corn oil, $\varepsilon_f = 2.87$, were measured using the standard technique of dielectric spectroscopy in a low electric field ~ 4 V/mm and the particle volume fractions c in the suspensions used for these measurements varied from 1% to 15%. The measurements were performed on a broadband dielectric spectrometer (BDS)-80 (Novocontrol, GmBH, Hundsangen, Germany) in the frequency range from 1 Hz to 3 MHz. The dielectric sample cell consisted of a round plate capacitor (20 mm in diameter) filled with a suspension and the cell constant was determined with pure hexadecane (Aldrich Chemical Co., St. Louis, MO, 99%). During the measurements, the temperature of the cell was controlled at 22.0 ± 0.05 °C. Then following the procedure proposed in Refs. [13,14] the value of β for the particles was calculated using the Maxwell-Wagner expression for the concentration dependence of ε_s^* for a suspension of randomly distributed spheres [17,18]

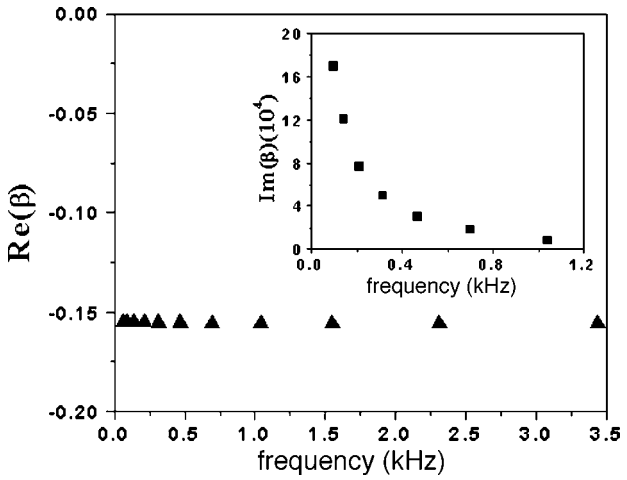

FIG. 1. The frequency dependence of the particle polarizability for a suspension of polyolefin particles in corn oil.

$$(\varepsilon_s^* - \varepsilon_f^*)/(\varepsilon_s^* + 2\varepsilon_f^*) = c\beta. \tag{2}$$

The value Re(β) was found to equal -0.15 over the frequency range 0.1–3.5 kHz used in our experiments whereas Im(β) was found to decrease rapidly with frequency from 1.8×10^{-3} for 0.1 kHz to less than 2×10^{-4} for frequencies greater than 1 kHz (Fig. 1).

B. Electric chamber

The experiments were performed in a horizontal parallel-plate chamber (6 cm wide, 12 cm long, and 3 mm high) [Fig. 2(a)]. The bottom of the Plexiglas chamber was equipped with 16 linear, flat, brass electrodes (1.6 mm wide and 11 cm long) having smoothed edges, which were embedded into 1.6-mm-deep grooves at 2 mm intervals. The electrodes were alternately connected to the high voltage and to the ground. The top of the chamber, consisting of a transparent glass coated with a conducting layer of indium tin oxide (ITO), was grounded. A Teflon spacer was used to keep a gap between the chamber top and bottom. The chamber was illuminated through the transparent top plate using a spread beam light source. The particle segregation was recorded through the top by a digital camera fixed above the chamber. The applied ac field, the amplitude and frequency of which varied from 1 to 5 kV rms (root mean square) and 0.1 to 3 kHz, was produced with a high-voltage amplifier (model 10/40, Trek Inc., Medina, NY). These frequency and voltage ranges were selected in order to suppress the effects of electroconvection and ac-field electrophoresis.

To indicate the trend of the field-induced particle motions in the chamber, we solved Laplace's equation and computed the spatial distribution of the field strength generated inside the chamber using a numerical procedure described in Ref. [14]. Since the gap between the electrodes was small compared to the length of the channel, the electric field was taken

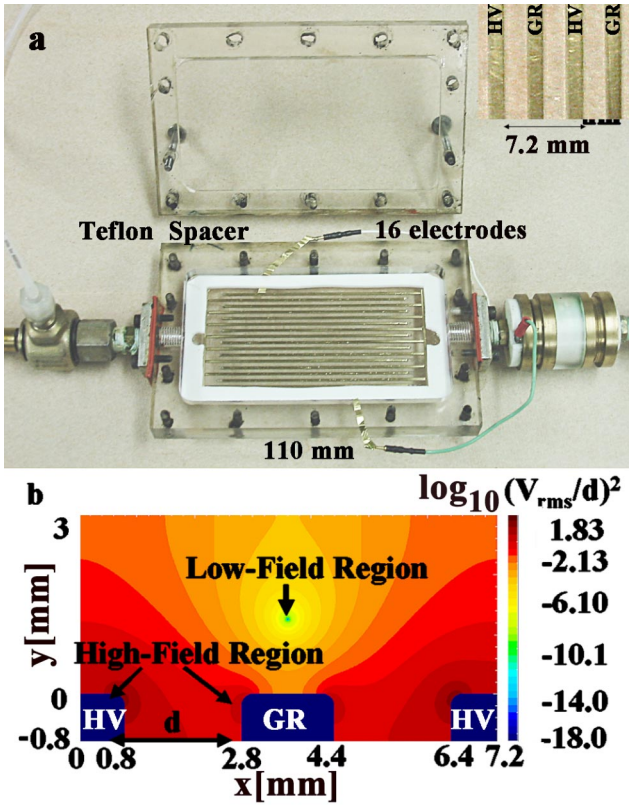

FIG. 2. (Color online) (a) Dielectrophoretic chamber, having 16 electrodes and teflon spacer used to maintain gap of 3 mm above the electrodes. Inset shows top view of the four electrodes along with dimensions; HV and GR refer to the high-voltage and grounded electrodes, respectively. (b) The distribution of the square of the field strength, E^2 (expressed in units of V_{rms}^2/d^2 in base-10 logarithmic scale), for a pair of electrodes. Half of the high-voltage electrodes are on the left ($0 \leqslant x \leqslant 0.8$) and on the right ($6.4 \leqslant x \leqslant 7.2$) and the grounded electrode is in the middle ($2.8 \leqslant x \leqslant 4.4$). The top ($y = 3.0$) is also grounded.

as two dimensional, varying only along the channel cross section in the x and y directions. As a result of the symmetry and periodicity of the electrode array along the x direction, the field was computed only within a periodic cell containing a pair of electrodes [Fig. 2(a)]. The corn oil and channel bottom plate were assumed to form a continuous medium because of their similar dielectric properties. Following [14], an insulating electrical boundary condition was imposed along the bottom boundary of the computational cell between the electrodes. The distribution of the field strength in a channel cross section is depicted in Fig. 2(b). Notice the appearance of two regions of high field strength near the electrode edges and a wide region of low strength above the center of the grounded electrode near the midplane of the channel, in which the negatively polarized particles are expected to accumulate.

C. Procedure

The suspensions were freshly prepared before each experiment and were continuously stirred for ~30 min with a magnetic stirrer to disperse the particles uniformly. The suspension thus formed was kept for about 2 h to allow those few particles which were either heavier or lighter than the fluid to settle down or float on the surface, and only that fraction of the suspension consisting of neutrally buoyant particles was used in the experiments. This suspension was then pumped into the chamber at a very low flow rate to prevent trapping air bubbles inside. Once the chamber was filled without any air being trapped within it, the flow was stopped and an ac electric field was applied. Typical experiments lasted about 30–90 min. Once the experiment was completed, the chamber was flushed with pure corn oil and the electrodes were gently cleaned.

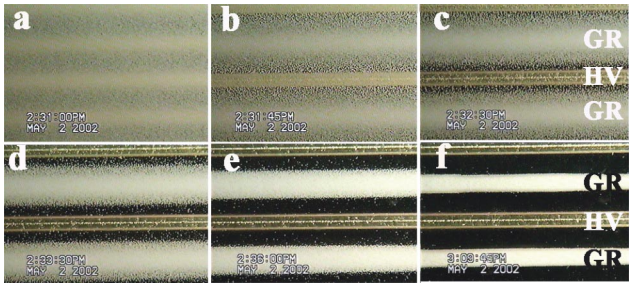

FIG. 3. (Color online) The particle distribution in a suspension with 10% (v/v) particle concentration (a) before and (b)–(f) following the application of a field 5 kV rms, 100 Hz at $t =$ (b) 45 s, (c) 90 s, (d) 150 s, (e) 300 s, and (f) final state, ~39 min. The electrode width is 1.6 mm. HV and GR refer to the high-voltage and grounded electrodes, respectively.

III. EXPERIMENTAL DATA

The photographs presented in Fig. 3 show the time evolution of the particle distribution in the 10% (v/v) suspension following the application of the electric field of 5 $\mathrm{kV_{rms}}$ and 0.1 kHz. The particles (seen as white spots in the photos) were initially uniformly distributed [Fig. 3(a)]. As expected, the dielectrophoretic force, Eq. (1), caused the particles to move from the regions of high field strength toward the regions of low strength [Fig. 2(b)]. It took about 45 s for the particles, which were initially located near the high-voltage electrodes, to move away so that the electrodes became visible [Fig. 3(b)]. Following the 90-s exposure to the applied field, most of the particles traveled along the channel cross section from the regions near the high-voltage electrodes toward the low-field region above the grounded electrode [Fig. 3(c)]. After about 150 s a distinct front between the suspension and the suspending fluid containing very few particles [Fig. 3(d)] was formed along the channel. As time progressed, the front slowly moved away from the high field regions and the particles became progressively confined to a thin column above the grounded electrode [Fig. 3(e)]. After a sufficiently long exposure to the field, ~1 h, nearly all the particles accumulated in the region above the grounded electrode, and the concentration front stopped moving. At that point the experiment was terminated given that no further changes could be discerned [Fig. 3(f)].

A similar type of field-driven particle redistribution was observed in suspensions having particle concentrations 5%, 10%, and 15% (v/v) and the photographs presented in Fig. 4

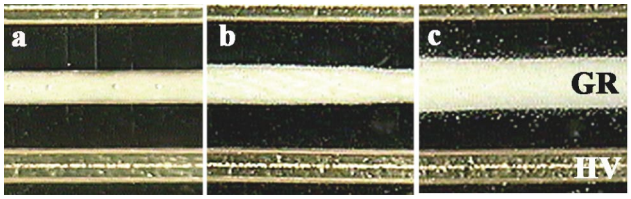

FIG. 4. (Color online) The final position of the concentration front in suspensions with (a) 5%, (b) 10%, and (c) 15% (v/v) particle concentrations following the application of a field 5 kV_{rms}, 100 Hz. Exposure times: (a) 41 min, (b) 38 min, and (c) 30 min. The electrode width is 1.6 mm. HV and GR refer to the high-voltage and grounded electrodes respectively.

demonstrate the final location of the concentration fronts for these suspensions. The sharpness of the front, as seen from the top of the channel, was found to be increasing with an increase in the magnitudes of the applied ac voltage and of the frequency (Fig. 5). We found that the use of the characteristic time for dielectrophoresis [13,14] τ_d, Eq. (3), makes it possible to combine the data on the time dependence of the front position for different voltages and frequencies into one band for $t/\tau_d \leqslant 20$ (Fig. 6). Here,

$$\tau_d = \frac{3d^4\eta_f}{a^2\varepsilon_0\varepsilon_f|\mathrm{Re}(\beta)|V_{rms}^2}, \tag{3}$$

where η_f is the viscosity of the suspending fluid, d is the electrode width, a is the particle radius, and V_{rms} is the root mean square of the applied ac voltage.

Note that a distinct concentration front, as seen in Fig. 4, does not form in dilute suspensions. This is evident from the photos presented in Fig. 7(a) which depict the redistribution of the particles in the 0.1% (v/v) suspension following a 90-s exposure to the applied field of 5 kV_{rms} and 0.1 kHz. Here the particles are seen to accumulate above the grounded electrodes and to form a poorly defined undulating boundary between the suspension and the suspending fluid along the channel. Also, as can be seen from the photos in Figs. 3 and 4, another feature of the concentrated suspensions, $\sim 5\% - 15\%$ (v/v), is the appearance of a thin stripe of particles in the region of high-field strength along the centerline of the high-voltage electrode, where they should have been repelled by the dielectrophoretic force, Eq. (1). The stripe is

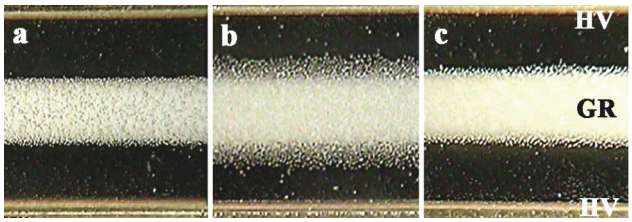

FIG. 5. (Color online) The effect of the field strength and frequency on the front sharpness in a suspension with 10% (v/v) particle concentration: (a) 5 kV_{rms}, 100 Hz, $t=20.5$ min, $t/\tau_d=63.4$; (b) 3 kV_{rms}, 100 Hz, $t=54.5$ min, $t/\tau_d=60.8$; and (c) 3 kV_{rms}, 2 kHz, $t=52.5$ min, $t/\tau_d=58.6$. The electrode width is 1.6 mm. HV and GR refer to the high-voltage and grounded electrodes, respectively.

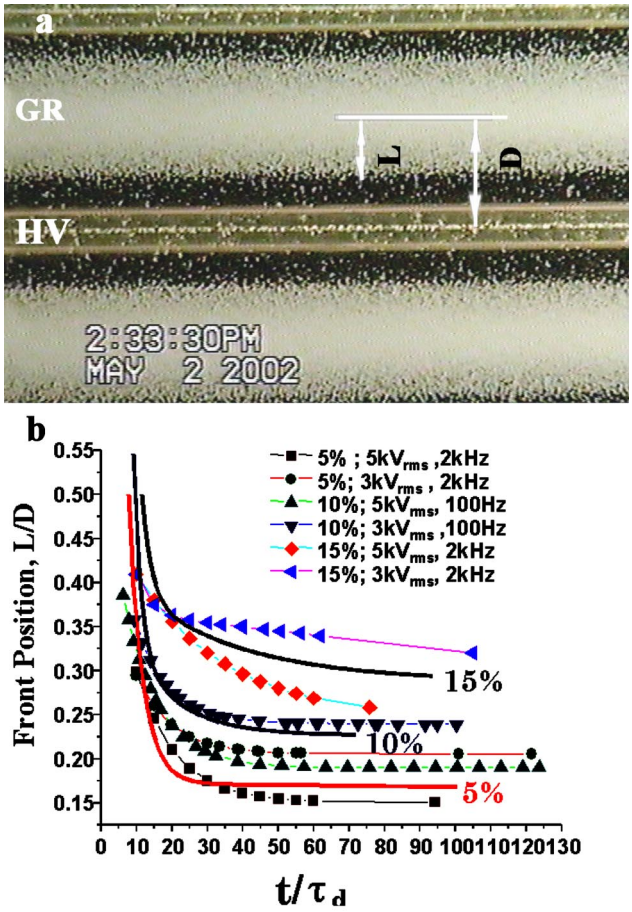

FIG. 6. (Color online) (a) The photograph illustrates how the front position L was measured; HV and GR refer to the high-voltage and grounded electrodes, respectively; $D=3.6$ mm. (b) The experimental data (symbols) and computational results (solid lines) of the electrohydrodynamic model presented in Sec. IV B for the front propagation in suspensions with 5%, 10%, and 15% (v/v) particle concentrations for different voltages and frequencies of the applied fields. The experimental data and the simulation results are plotted against a nondimensional time, t/τ_d, with τ_d given by Eq. (3).

roughly one particle thick and two or three particles wide. Its width was found to depend on the polishing of the electrodes and to increase slightly with an increase in the initial particle concentration of the suspension. Such an accumulation of the particles in that region was not observed in dilute suspensions, $\sim 0.01\% - 0.2\%$ (v/v) [13].

IV. THEORY OF ac DIELECTROPHORETIC PHENOMENA

A. Thermodynamics

In Refs. [19–21], we developed a theory for the free energy of a suspension of polarized spherical particles subject to an ac electric field, $\mathbf{E}=\mathbf{E}_0(r)\cos\omega t$, which is based on the Maxwell-Wagner model for the interfacial polarization of a particle and the Lorentz-Lorenz model for the local field acting on a particle. This theory yields the following expres-

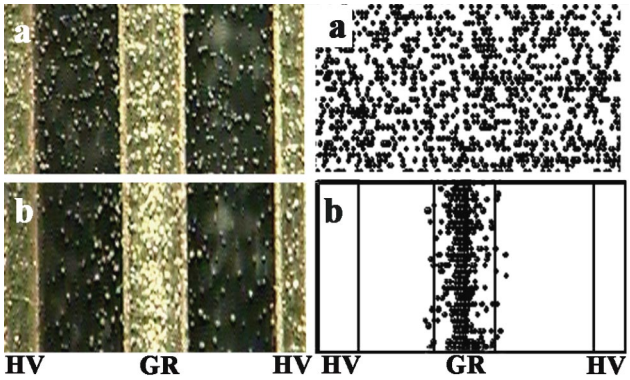

FIG. 7. (Color online) The photographs in the left illustrate the particle distribution in a suspension with 0.1% (v/v) particle concentration (a) before and (b) following the application of a field 5 kV_{rms} and 100 Hz for 90 s. The electrode width is 1.6 mm. The pictures on the right present the numerical simulations of the particle distribution (a) before and (b) following the application of a field 5 kV_{rms} and 100 Hz for 90 s which use a single-particle model. HV and GR refer to high-voltage and grounded electrodes, respectively.

sions for the chemical potential μ_p and the osmotic pressure Π_p of the particles averaged over the period of the field oscillations:

$$\mu_p = \frac{k_B T}{v_p}\frac{df_0}{dc} - \varepsilon_0 \left(\frac{\partial \varepsilon_s'}{\partial c}\right)_{\omega t_c} \left\langle \frac{\mathbf{E}^2}{2} \right\rangle,$$

with

$$f_0 = c \ln\frac{c}{e} + c\int_0^c \frac{Z(c)-1}{c} dc,$$

$$\Pi_p = \frac{k_B T}{v_p} cZ + \varepsilon_0 \left[\varepsilon_s' - c\left(\frac{\partial \varepsilon_s'}{\partial c}\right)_{\omega t_c} \right] \left\langle \frac{\mathbf{E}^2}{2} \right\rangle, \tag{4}$$

where $k_B T$ is the thermal energy, c is the particle volume fraction, Z is the suspension compressibility factor, and $(\partial \varepsilon_s'/\partial c)_{\omega t_c}$ is the derivative of the real part of the complex dielectric permittivity of the suspension, ε_s^*, taken at a constant value of ωt_c with t_c being the relaxation time of the dielectric phenomena [20]. The first term in Eqs. (4) refers to the free energy and the osmotic pressure of the particles in the absence of the electric field whereas the other represents the field contribution caused by the interaction of the particles with the field as well as the interparticle dipolar interactions. The concentration dependence of the compressibility factor was described by the Carnahan-Starling equation for a suspension of spheres in the disordered state [17] $Z=(1+c+c^2-c^3)/(1-c)^3$ when $0<c\leqslant 0.5$ and by $Z\approx A/(c_m-c)$ with $A\sim 1.85$ as $c\to c_m$, where $c_m\sim 0.63-0.64$ denotes the concentration of the spheres at random close packing. The Maxwell-Wagner expression, Eq. (2), was used to compute ε_s^* in the second term of Eq. (4). When $\mathrm{Im}(\beta)$ is small (which is the case for our experiments), Eq. (2) yields

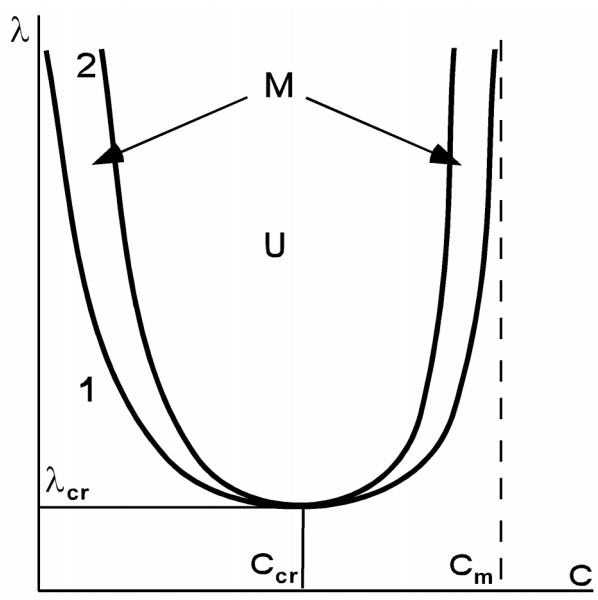

FIG. 8. The phase diagram of the ''particle concentration vs the field strength'' of suspensions subjected to electric fields: the metastable and unstable domains are denoted by *M* and *U*, respectively, λ is the relative strength of the field, and *c* is the particle volume concentration (Ref. [20]); 1 and 2 are the coexistence curve and spinodal, respectively.

$$\left(\frac{\partial \varepsilon_s}{\partial c}\right)_{\omega t_c} \approx \frac{3\varepsilon_f \mathrm{Re}(\beta)}{[1-c\,\mathrm{Re}(\beta)]^2}. \tag{5}$$

The phase diagram of the ''particle concentration versus the field strength'' of a suspension subject to a spatially uniform ac electric field predicted by Eq. (4) predicts [19,20] in terms of c and $\lambda = \varepsilon_0 \varepsilon_f \langle E^2 \rangle v_p / k_B T$ being a measure of the relative field strength, appears to be similar to the ''concentration versus temperature'' phase diagrams for the first-order phase separation in a mixture of two liquids which are completely miscible only above a certain temperature. As an example, the simplest suspension phase diagram [20] is sketched in Fig. 8 where M and U denote the metastable and unstable domains, respectively. The random arrangement of the particles becomes unstable when

$$\frac{\partial \mu_p}{\partial c} = 0, \tag{6}$$

which represents the spinodal curve in the equilibrium phase diagram (Fig. 8). The critical point on the spinodal curve, c_{cr} and λ_{cr}, coincides with the inflection point of μ_p as a function of c so that

$$\frac{\partial \mu_p}{\partial c} = \frac{\partial^2 \mu_p}{\partial c^2} = 0. \tag{7}$$

The one-phase region of the phase diagram includes the random spatial arrangement of the particles, whereas the two-phase region (at $\lambda_{cr} \geqslant \lambda$) corresponds to the appearance of a field-induced phase separation (Fig. 8). On the coexistence

curve the values of the chemical potential and of the osmotic pressure of the particles in the coexisting phases having particle concentrations c_1 and c_2, respectively, are equal thereby leading to the following relations:

$$\mu_{\mathrm{p}}(c_1)=\mu_{\mathrm{p}}(c_2), \quad \Pi_p(c_1)=\Pi_p(c_2). \tag{8}$$

The phase diagram depicted in Fig. 8 corresponds to the case of small $\mathrm{Im}(\beta)$ [20] for which $c_1\to 0$ and $c_2\to c_{\mathrm{m}}$ for $\lambda \to\infty$.

The phase diagrams of the ''particle concentration versus the field strength'' given by Eqs. (4) and (6)–(8) provide a consistent interpretation of the available experimental data on the field-induced aggregation phenomena in electrorheological fluids and aqueous suspensions [19,20]. In Ref. [21], we considered a quasiequilibrium spatial distribution of the particle concentration caused by dielectrophoresis in a suspension subject to a spatially nonuniform ac field that would have been reached when the chemical potential of a particle becomes independent of position so that

$$\nabla\mu_{\mathrm{p}}[c(\mathbf{r}),\langle\mathbf{E}^2(\mathbf{r})\rangle]=0. \tag{9}$$

Equation (9) represents c as a function of $\langle\mathbf{E}^2\rangle$ along the curve $\mu_{\mathrm{p}}=\mathrm{const}$ on the suspension phase diagram, Fig. 8. It was found [21] that, under certain conditions, this curve would cross the coexistence curve, Eqs. (8). In this case, dielectrophoresis was predicted to be accompanied by a phase separation leading to an abrupt change in the spatial particle concentration distribution and, as a result, to the formation of a concentrated layer of particles in those regions where, depending on the sign of the particle polarizability, the strength of the electric field is either high or low. This prediction is qualitatively consistent with the formation of the concentration front observed in the photos of Figs. 3 and 4. We now wish to generalize the thermodynamic theory [19–21] and consider the kinetics of the front formation and propagation.

B. Electrohydrodynamic model

A theory should encompass the field and flow equations for both the one-phase as well as the two-phase states of a suspension where the one-phase or two-phase equations should be used depending on whether the point representing the local values of the particle concentration and of the electric field in the suspension phase diagram, Fig. 8, is located below or above the coexistence curve, respectively. First, let us consider the equations for the one-phase region for which $\partial\mu_{\mathrm{p}}/\partial c>0$. Since the time scale of hydrodynamic phenomena is significantly larger than the period of the field oscillations, we can average the equations for the suspension flow over the field oscillations. Next, because of the small suspension velocity, we can neglect any difference between the electromagnetic fields in the laboratory system and in the instantaneous reference system moving with a suspension. Furthermore, we limit our analysis to the case when any magnetic effects associated with a time varying electric field are negligible. Under these conditions, we can employ the quasisteady electrodynamic equations [22,23]. Written in terms of the Fourier components of the electric field, $\mathbf{E}^*_\omega(\mathbf{r})$, and the electric displacement, $\mathbf{D}^*_\omega(\mathbf{r})$, these equations take the form

$$\nabla\cdot\mathbf{D}^*_\omega(\mathbf{r})=0, \quad \nabla\times\mathbf{E}^*_\omega(\mathbf{r})=0, \tag{10}$$

with

$$\mathbf{D}^*_\omega=\varepsilon_0[\varepsilon'_{\mathrm{s}}(\omega,c)-\mathrm{i}\varepsilon''_{\mathrm{s}}(\omega,c)]\mathbf{E}^*_\omega,$$

where $\varepsilon^*_{\mathrm{s}}=\varepsilon'_{\mathrm{s}}(\omega,c)-\mathrm{i}\varepsilon''_{\mathrm{s}}(\omega,c)$ is the complex dielectric permittivity of a suspension. Equations (10) lead to Laplace's equation for the complex Fourier component of the electric potential φ^*_ω:

$$\nabla\cdot[\varepsilon^*_{\mathrm{s}}(\omega,c)\nabla\varphi^*_\omega]=0, \tag{11}$$

where

$$\mathbf{E}^*_\omega=-\nabla\varphi^*_\omega.$$

For the concentration dependence of $\varepsilon^*_{\mathrm{s}}$, we use Eq. (2) in which the frequency dependence of $\beta(\omega)$ is taken from measurements at low electric fields. The spatial variation of $\varepsilon^*_{\mathrm{s}}(\omega,c)$ in Eq. (11) is caused by the spatial variation of the particle concentration c due to their motion following the application of a spatially nonuniform ac electric field.

The equations for the suspension flow averaged over the field oscillations include the continuity equation

$$\nabla\cdot\mathbf{v}=0, \tag{12}$$

the momentum balance equation

$$\rho_{\mathrm{s}}\left(\frac{\partial\mathbf{v}}{\partial t}+\mathbf{v}\cdot\nabla\mathbf{v}\right)=-\nabla p+\nabla\cdot\boldsymbol{\sigma}^{\mathrm{vis}}-c\nabla\mu_{\mathrm{p}}+c(\rho_{\mathrm{p}}-\rho_{\mathrm{f}})\mathbf{g}, \tag{13}$$

and the continuity equation for the particles,

$$\frac{\partial c}{\partial t}+\nabla\cdot(c\mathbf{v}+\mathbf{j}_{\mathrm{p}})=0, \tag{14}$$

where $\mathbf{v}$ is the bulk velocity of the suspension, $\rho_{\mathrm{s}}=(1-c)\rho_{\mathrm{f}}+c\rho_{\mathrm{p}}$ is the suspension density with ρ_{p} and ρ_{f} being the densities of the particles and of the fluid, $\mathbf{g}$ is the gravitational acceleration, p is the pressure, $\boldsymbol{\sigma}^{\mathrm{vis}}$ is the viscous stress tensor, and $\mathbf{j}_{\mathrm{p}}$ is the particle flux in the reference system moving with the suspension. The fourth term on the right-hand side of Eq. (13) is the bulk gravity force which vanishes for neutrally buoyant particles whereas the term $-c\nabla\mu_{\mathrm{p}}$, with μ_{p} being given by Eq. (4) with $\langle\mathbf{E}^2\rangle=\frac{1}{2}|\mathbf{E}^*_\omega(\mathbf{r})|^2$, represents the bulk electric force exerted on a suspension by an applied ac field. Careful analysis indicates that this approximation for the bulk electric force is appropriate when $|\mathrm{Im}(\beta)|\ll|\mathrm{Re}(\beta)|$. For a spatially uniform particle concentration, the bulk electric force equals the total force exerted on the particles per unit volume of the suspension, so that, on account of Eq. (4), we obtain

$$-c\nabla\mu_{\mathrm{p}}|_{c=\mathrm{const}}=n\mathbf{F}_{\mathrm{dep}}, \tag{15}$$

with

$$\mathbf{F}_{\mathrm{dep}}=\frac{\varepsilon_0 v_{\mathrm{p}}}{2}\left(\frac{\partial \varepsilon_{\mathrm{s}}'}{\partial c}\right)_{\omega t_{\mathrm{c}}}\nabla\langle \mathbf{E}^2\rangle,$$

where n is the number density of the particles and $\mathbf{F}_{\mathrm{dep}}$ is the dielectrophoretic force exerted on a single particle in a suspension. Since $(\partial\varepsilon_{\mathrm{s}}'/\partial c)_{\omega t_{\mathrm{c}},c}\to 3\varepsilon_{\mathrm{f}}\,\mathrm{Re}(\beta)$ for $c\to 0$, Eq. (15) for $\mathbf{F}_{\mathrm{dep}}$ generalizes the expression, Eq. (1), for the dielectrophoretic force by accounting for the effect of the other particles on the magnitude of the local field acting on a test particle in a suspension.

We restrict our consideration to the specific case of low particle Reynolds numbers and relatively high particle Peclet numbers associated with a weak Brownian diffusion of the particles, which is relevant to our current experiments. To describe the flow, the suspension is viewed as an effective Newtonian fluid with a concentration-dependent viscosity [24]. In this approach, the hydrodynamic interactions of the particles subjected to shear are incorporated through the concentration dependence of the suspension viscosity and the hindrance function in the expression for the particle velocity relative to the suspending fluid [24]. Under these conditions, the equations for the effective viscous stress and the particle flux become

$$\sigma_{ij}^{\mathrm{vis}}=\eta_{\mathrm{s}}(c)\left(\frac{\partial v_i}{\partial x_j}+\frac{\partial v_j}{\partial x_i}\right),$$

$$\mathbf{j}_{\mathrm{p}}=\frac{c(1-c)^2 v_{\mathrm{p}}}{6\pi a\,\eta_{\mathrm{s}}(c)}[-\nabla\mu_{\mathrm{p}}+(\rho_{\mathrm{p}}-\rho_{\mathrm{f}})\mathbf{g}], \tag{16}$$

where $\eta_{\mathrm{s}}=\eta_{\mathrm{f}}\hat{\eta}(c)$ is the suspension viscosity, with η_{f} being the suspending fluid viscosity and $\hat{\eta}=[1+1.5c/(1-c/c_{\mathrm{m}})]^2$ the Leighton-Acrivos expression for the concentration dependence of the suspension viscosity [24], and the factor $(1-c)^2$ in the expression for the particle flux represents the hindrance function [24]. The hydrodynamic equations (12)–(14) and (16) are coupled with the electrodynamic equations (10) and (11) through the field dependence of μ_{p} for the former and the concentration dependence of $\varepsilon_{\mathrm{s}}^*$ for the latter.

For the limiting case of a dilute suspension, for which $c\to 0$ and $\partial f_0/\partial c\to 1/c$, Eqs. (10)–(13) reduce to the field and flow equations for the suspending fluid while Eqs. (4), (14), and (16) yield

$$\frac{\partial c}{\partial t}+\nabla\cdot[c(\mathbf{v}+\mathbf{u}_{\mathrm{e}})]=D_{\mathrm{B}}\Delta c, \tag{17}$$

with

$$\mathbf{u}_{\mathrm{e}}=\frac{v_{\mathrm{p}}}{6\pi a\,\eta_{\mathrm{f}}}\left[\frac{3}{2}\varepsilon_0\varepsilon_{\mathrm{f}}\,\mathrm{Re}(\beta)\nabla\langle\mathbf{E}^2\rangle+(\rho_{\mathrm{p}}-\rho_{\mathrm{f}})\mathbf{g}\right],$$

where $\mathbf{u}_{\mathrm{e}}$ is the velocity of a particle relative to the suspending fluid under the action of the dielectrophoretic, Eq. (1), and gravity forces, and $D_{\mathrm{B}}=k_{\mathrm{B}}T/6\pi a\,\eta_{\mathrm{f}}$ is the particle Brownian diffusion coefficient. When Brownian effects are insignificant, Eq. (17) leads to the single-particle model

$$\frac{\partial c}{\partial t}+\nabla\cdot[c(\mathbf{v}+\mathbf{u}_{\mathrm{e}})]=0, \tag{18}$$

which was found [13,14] to be consistent with the experimental data for dilute suspensions of negatively and positively polarized particles subject to a high-gradient ac field ($\sim$kV/mm) and shear even though the value of the particle polarizability, $\beta(\omega)$, was measured at low-strength fields ($\sim$V/mm). Another limiting case is the quasiequilibrium state of a suspension of neutrally buoyant particles subject to a spatially nonuniform ac field, for which Eqs. (4) and (12)–(16) yield $\mathbf{v}=0$ and $\nabla p=0$ while the particle distribution satisfies Eq. (9).

Next, we generalize the electrohydrodynamic model, Eqs. (4) and (10)–(16), to the two-phase region of the suspension phase diagram, Fig. 8. Notice that these equations appear to be unstable within the unstable domain U in the phase diagram (Fig. 8) since $(\partial\mu_{\mathrm{p}}/\partial c)_{\mathrm{E}}<0$. We limit our analysis to the case when the field-induced phase separation occurs significantly faster than typical hydrodynamic phenomena, thereby allowing us to use a quasiequilibrium approximation for the local values of the particle concentration and of the electric field in the two-phase region. In this case, the value of the chemical potential is the same in both phases and is specified by the coexistence curve, Eqs. (8), in the phase diagram as a function of λ, i.e., $\mu_{\mathrm{p}}=\mu_{\mathrm{p}}(\lambda)$. The particle concentrations in both phases, c_1 and c_2, are also specified by the coexistence curve, Eqs. (8), as functions of λ, whereas the volume fraction of the high concentration phase, ψ, is given by the lever rule, $c_2\psi+c_1(1-\psi)=c$, as a function of c and λ. Within this approximation, the two-phase state of the suspension is viewed as a ''mushy'' zone. For simplicity, the complex dielectric permittivity, the viscosity, and the hindrance function for this zone are assumed to be determined only by the total particle concentration c through the use of the same functions as those for the one-phase region, even though they are in fact functions of both c and ψ. Under these conditions, the two-phase model consists of Eqs. (10)–(14) and (16) in which the chemical potential is now specified as a function of the field strength, $\mu_{\mathrm{p}}=\mu_{\mathrm{p}}(\lambda)$, through solving Eqs. (8).

Equations (10)–(14) and (16) are subject to the standard boundary and initial conditions for the quasisteady electrodynamic [22,23] and flow equations [24] which, in line with our experiments where the ac field was applied at time $t=0$, become

$$[\mathbf{E}_{\omega,\mathrm{II}}^*]_S=\mathbf{0},\quad [\mathbf{D}_{\omega,\perp}^*]_S=\mathbf{0},\quad \mathrm{Re}(\varphi_\omega^*|)_{S_{\mathrm{el}}}=\varphi_{\mathrm{el}},$$

$$\mathrm{Im}(\varphi_\omega^*|)_{S_{\mathrm{el}}}=0, \tag{19}$$

$$\mathbf{v}|_S=\mathbf{0},\quad \mathbf{j}_{\mathrm{p},\perp}|_S=\mathbf{0},\quad \mathbf{v}|_{t=0}=\mathbf{0},\quad c|_{t=0}=c_0, \tag{20}$$

where the brackets denote the change in the respective variable along the tangential (II) and normal ($\perp$) directions to the

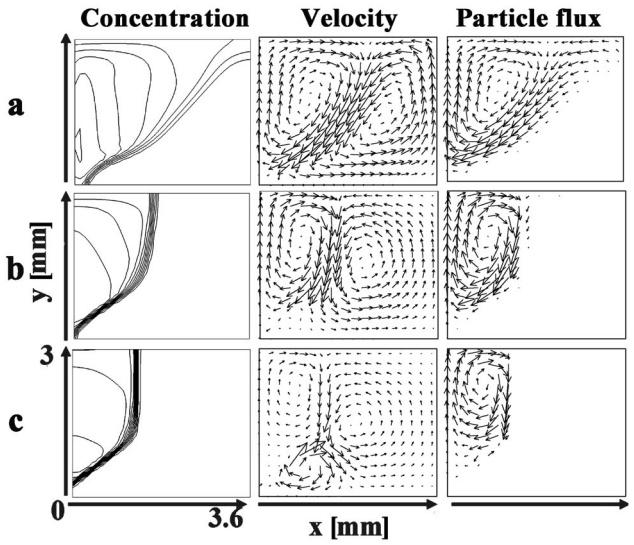

FIG. 9. Numerical simulations of the concentration contours, the suspension velocities, and the particle fluxes for the 10 (v/v)% suspension under the action of a field of 5 kV_{rms} and 100 Hz. Time is (a) 1 min, (b) 5 min, and (c) 20 min. The computed values for c_{max} in the low-field region [in %(v/v)] are (a) 40.3, (b) 54.7, and (c) 60.9. The arrows show the relative magnitudes of the suspension velocities and the particle fluxes, respectively. In (a)–(c), the maximum values for v_{max} are (a) 45.1 μm/s, (b) 5.7 μm/s, and (c) 1.6 μm/s and the maximum values for $(cv+j_p)_{max}$ are (a) 0.123 μm/s, (b) 0.019 μm/s, and (c) 0.003 μm/s]. Half of the grounded (GR) and high-voltage electrodes (HV) are on the left ($0 \leqslant x \leqslant 0.8$ mm) and on the right (2.8 mm$\leqslant x \leqslant$3.6 mm), respectively. The top ($y=3.0$ mm) is also grounded.

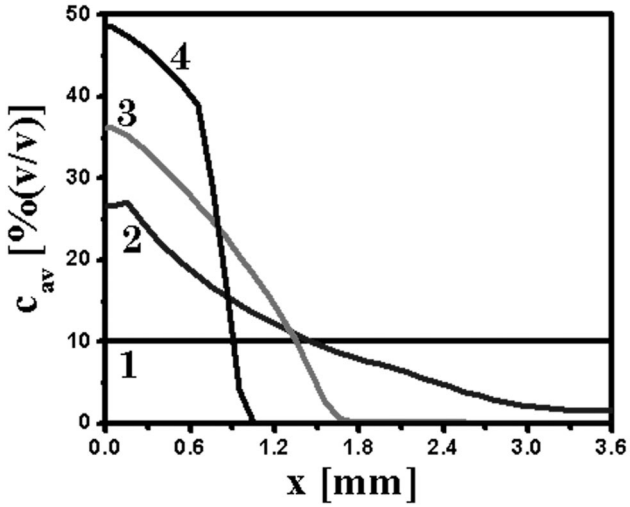

FIG. 10. The computed time variation of the particle concentration profile averaged along the vertical direction, c_{av}, for the 10 (v/v)% suspension following the application of a field of 5 kV_{rms} and 100 Hz. Locations $x=0$ mm and $x=3.6$ mm correspond to the centers of the adjacent ground (GR) and high-voltage (HV) electrodes, respectively. 1–4 correspond to concentration profiles at time=0, 45, 150, and 2370 s, respectively.

channel wall S, $\varphi_{el}\cos\omega t$ is the potential applied at the electrode surface S_{el}, and c_0 is the initial particle concentration.

V. SIMULATION RESULTS AND COMPARISON WITH EXPERIMENTS

The simulations were conducted using the data on the fluid and particle properties reported in Sec. II. For the 0.1% (v/v) suspension, we employed the single-particle model [13,14], which is equivalent to the set of equations (11) with $\varepsilon_s^* \equiv \varepsilon_f$, Eq. (18) with $\mathbf{v} \equiv 0$, under the appropriate boundary conditions, Eqs. (19) and (20). The pictures presented in Fig. 7(b) show the computed motions of the particles, being initially randomly distributed, under the action of the ac field of 5 kV_{rms} and 0.1 kHz. As can be seen from Fig. 7(b), the particles move toward the low-field region but do not form the distinct concentration front along the channel, which is in line with our observations for dilute suspensions [Fig. 7(a)].

The simulations for the 5%–15% (v/v) suspensions were conducted using the electrohydrodynamic model, Eqs. (10)–(14) and (16). The field-driven suspension flow was computed only within a periodic cell containing halves of the high-voltage and grounded electrodes [Fig. 2(b)] with the appropriate boundary conditions, Eqs. (19) and (20). The pictures presented in Fig. 9 show the computed evolution of the concentration distribution along the channel cross section following the application of the ac field of 5 kV_{rms} and 0.1 kHz to the 10% (v/v) suspension at $t=0$. After 5 min, the region above the high-voltage electrode appears to be nearly free of particles (i.e., $c \approx 0$), whereas the concentration in the region above the ground electrode is gradually increasing, forming a distinct front, which agrees well with the experimental observations for concentrated suspensions (Fig. 3). The pictures presented in Fig. 9 indicate that the field-induced particle redistribution is accompanied by the formation of two vortices in the channel cross section separated by the concentration front. The suspension flows clockwise in the particle enriched and counterclockwise in the region which has been depleted of particles. Depicted in Fig. 9 are the variations of the suspension velocity and of the total particle flux, $c\mathbf{v}+\mathbf{j}_p$, which demonstrate that the convective term dominates, causing the particles to move mainly along the flow streamlines. As a result, only the particles close to the concentration front travel with the front toward the low-field region due to the presence of the component of $\mathbf{j}_p$ directed perpendicular to the front. Simulations showed that due to the relatively low magnitude of the particle polarization, $|\beta| \sim 0.15$, changes of the electric field caused by the particle redistribution were within 10%–30% and were mainly located in the region close to the concentration front. Thus for our experimental conditions, the field distribution away from the front region remained unaltered from that depicted in Fig. 2.

To compare the theoretical predictions with the experimental data, the computed particle concentration profile was averaged along the vertical direction to obtain $c_{av} = (1/h)\int_0^h c(x,y,t)dy$ which characterizes the particle distribution as seen on a photograph taken through the channel top. As an example, the plots presented in Fig. 10 illustrate the computed time variation of c_{av} between the centers of the ground ($x=0$) and the adjacent high-voltage electrodes (x

$=3.6$ mm) for the 10% (v/v) suspension following the application of the electric field of 5 kV_{rms} and 0.1 kHz. We used such figures to simulate the position of the concentration front as a function of time for suspensions having particle concentrations 5%, 10%, and 15% (v/v) for the range of voltages and frequencies used in our experiments. As can be seen from Fig. 6(b), the simulation results for the propagation of the concentration front are in a reasonable agreement with experimental data for $t/\tau_d \leqslant 20$ even though the model contains no fitting parameters. As time progresses, the simulations of the front position are found to overestimate the data for the high voltages and frequencies and underestimate the data for the low voltages and frequencies. Also, the simulations do not predict that the front sharpness, as seen from the channel top (Fig. 5), increases with an increase in the magnitudes of the applied voltage and frequency. These drawbacks of the model might be related to the fact that ours is a continuum model which operates on scales substantially larger than the particle size. Also, this model ignores any electrophoretic phenomena the significance of which increase with a reduction in the magnitude and frequency of the applied voltage and neglects the field-induced solidlike behavior of concentrated suspensions (the appearance of yield stress, in particular) under the action of a strong electric field. As a result, the model, Eqs. (4) and (10)–(16), accounts for the influence of the field frequency on the particle motion only through the frequency dependence of the particle polarizability, $\beta(\omega)$.

VI. PARTICLE ACCUMULATION ON THE HIGH-VOLTAGE ELECTRODE

Using Laplace's equation and accounting for the symmetry and periodicity of the electrode array [Fig. 2(a)], we find that the electric potential near the high-voltage electrode, $y \to 0$, can be expressed as

$$\varphi \approx \sqrt{2} V_{\rm rms} \left[1 + Ay - \frac{y^3}{6} \frac{d^2A}{dx^2} + O(y^5) \right] \cos \omega t, \qquad (21)$$

where $A(x)$ is symmetric about the electrode center x_c. A numerical solution of Laplace's equation indicates that $A > 0$ and $d^2A/dx^2 > 0$ at $x = x_c$ [Fig. 2(b)]. Using Eq. (21), we therefore obtain that

$$\langle \mathbf{E}^2 \rangle \approx V_{\rm rms}^2 \{ A^2 + [(dA/dx)^2 - A d^2A/dx^2] y^2 \},$$

$$\langle E_y^2 \rangle \approx V_{\rm rms}^2 [A^2 - A(d^2A/dx^2) y^2]. \qquad (22)$$

Since $dA/dx \to 0$ for $x \to x_c$, the distribution of the field strength has a saddle point at x_c. Substitution of $\langle \mathbf{E}^2 \rangle$ into Eq. (1) yields the dielectrophoretic force acting on a particle near this point:

$$\mathbf{F}_{\rm dep} \approx 4 \varepsilon_0 \varepsilon_f \pi a^3 \, {\rm Re}(\beta) V_{\rm rms}^2 \left\{ \left[A \frac{dA}{dx} + \frac{1}{2} \left(\frac{dA}{dx} \frac{d^2A}{dx^2} - A \frac{d^3A}{d^3x} \right) y^2 \right] \mathbf{e}_x + \left[\left(\frac{dA}{dx} \right)^2 - A \frac{d^2A}{dx^2} \right] y \mathbf{e}_y \right\}. \qquad (23)$$

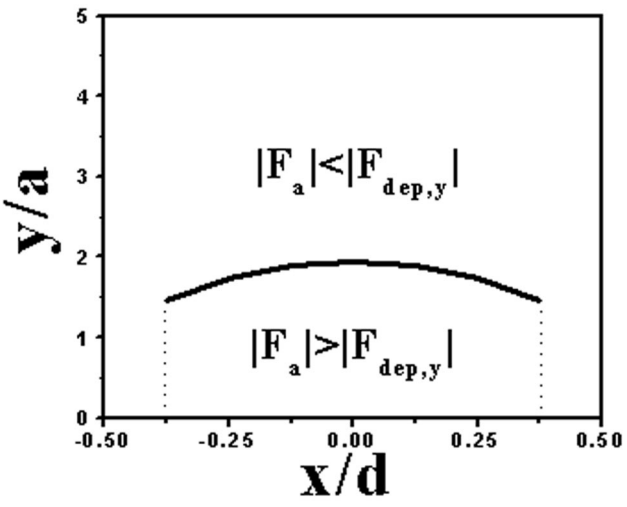

FIG. 11. The computed boundary of the region [defined by Eq. (24)] near the high-voltage electrode where the vertical component of the dipolar force exceeds the dielectrophoretic force. $x/d = 0.0,\ 0.5, -0.5$ refers to the center and the two edges of the high voltage electrode, respectively.

Polarized particles located near an electrode also experience an attraction force toward the electrode, which equals approximately the dipolar force between the particle and its image. The equation for this dipolar force [19], taking the case of a negligibly small imaginary component of β, yields the following expression for the attraction force acting on a particle whose center is located at the distance y from the electrode surface: $\mathbf{F}_a \approx -\pi \varepsilon_0 \varepsilon_f [{\rm Re}(\beta)]^2 \langle E_y^2 \rangle (3a^6/2y^4) \mathbf{e}_y$. Therefore, a particle will be trapped near the high-voltage electrode when the attraction force exceeds the y component of the dielectrophoretic force. Using Eqs. (22), we find that this condition is met for

$$3a^3 |{\rm Re}(\beta)| [A^2 - A(d^2A/dx^2) y^2] \geqslant 8y^5 [A(d^2A/dx^2) - (dA/dx)^2]. \qquad (24)$$

The region defined by Eq. (24) is independent of the applied voltage. Having the maximum height near the centerline of about one particle diameter, it occupies a thin layer near the surface of the high-voltage electrodes (Fig. 11), which constitutes about 0.45% of the channel volume. Following the application of an electric field, the x component of the dielectrophoretic force, Eq. (23), will cause the negatively polarized particles, which were initially located in this region, to move toward the centerline of the high-voltage electrode. When the number of these particles is sufficiently large they will form continuous stripes along the high-voltage electrodes. This explains the fact that such stripes are only observed for sufficiently concentrated suspensions. The characteristics of the particle accumulation along the centerlines of the high-voltage electrodes are qualitatively consistent with the experimental data reported in Sec. III. The prediction of the particle aggregation patterns on the high-voltage electrodes is well beyond the scope of the continuum model presented in Sec. IV, which operates on scales substantially larger than the particle diameter.

VII. SUMMARY AND CONCLUSIONS

We reported that when, concentrated suspensions of neutrally buoyant, negatively polarized particles were subjected to a high-gradient ac field, a distinct front was formed separating a suspension from a region of essentially particle-free fluid which moved away from the high-field regions and eventually confined the particles to a thin column in the low-field region. This phenomenon owed its existence to the interparticle electrical interactions. A theory was proposed for the front propagation which generalizes our earlier theory for the thermodynamics of the field-induced phase transitions in suspensions of polarized particles. The electrohydrodynamic model encompasses the coupled quasi-steady-field equations and the momentum and continuity balance equations for one- and two-phase states of a suspension, which are averaged over the field oscillations. The suspension is viewed as an effective Newtonian fluid with a concentration dependent effective viscosity. The bulk electric force exerted on a suspension and the particle velocity relative to the suspending fluid are expressed in terms of the chemical potential of the particles. Simulations were conducted using the data for the fluid and particle properties which were measured independently. The simulation results for the front propagation are quantitatively consistent with the experimental data even though the model contains no fitting parameters.

We also observed the appearance of a thin stripe, roughly one particle thick and two or three particles wide, in the region of the high-field strength, which should have been repelled from this region by the dielectrophoretic force. The formation of such a thin stripe in the high-field region was explained by considering the balance of the forces exerted on a particle located close to the high-voltage electrodes.

The results of our studies demonstrate that by combining field-induced dielectrophoresis and phase separation one can create a method for strongly concentrating particles in focused regions of a dielectrophoretic chamber. The proposed electrohydrodynamic model can simulate the basic characteristics of these coupled phenomena.

ACKNOWLEDGMENTS

The work was supported, in part, by grants from the National Aeronautics and Space Administration (Grant No. NAG3-2698) and the Defense Advanced Research Projects Agency through the Bioflips/Simbiosys Program, Mission Research Corporation/DARPA Contract No. DAAH01-02-R083. The measurements of the suspension complex permittivity and the particle size distribution were conducted using the instrumentation of the NJIT W.M. Keck Foundation Laboratory for the Electro-hydrodynamics of Suspensions.

[1] H. A. Pohl, *Dielectrophoresis: The Behavior of Natural Matter in Nonuniform Electric Fields* (Cambridge University Press, Cambridge, England, 1978).
[2] P. R. C. Gaskoyne and J. Vykoukal, Electrophoresis **23**, 1973 (2002).
[3] M. Koch, A. Evans, and A. Brunnschweiler, *Microfluidic Technology and Applications* (Research Studies Press, Baldock, England, 2000).
[4] T. B. Jones, *Electromechanics of Particles* (Cambridge University Press, Cambridge, England, 1995).
[5] C.-F. Chou, J. O. Tegenfeldt, O. Bakajin, S. S. Chan, E. C. Cox, N. Darnton, Th. Duke, and R. H. Austin, Biophys. J. **83**, 2170 (2002).
[6] Ch. L. Asbury, A. H. Diercks, and G. van den Engh, Electrophoresis **23**, 2658 (2002).
[7] R. Pethig, V. Bressler, C. Carswell-Crumpton, Y. Chen, L. Foster-Haje, M. E. Garcia-Ojeda, R. S. Lee, G. M. Talary, and K. M. Tate, Electrophoresis **23**, 2057 (2002).
[8] S. Tsukahara, K. Yamanaka, and H. Watarai, Chem. Lett. **3**, 250 (2001).
[9] R. Miles, Ph. Belgrader, K. Bettencourt, J. Hamilton, and S. Nasarabadi, Micro-Electro-Mech. Syst. **1**, 497 (1999).
[10] B. Malyan and W. Balachandran, J. Electrost. **51/52**, 15 (2001).
[11] L. Cui, D. Holmes, and H. Morgan, Electrophoresis **22**, 3893 (2001).
[12] *Handbook of Electrostatic Processes*, edited by J.-S. Chang, A. J. Kelly, and J. M. Crowley (Marcel Dekker, New York, 1995).
[13] A. Dussaud, B. Khusid, and A. Acrivos, J. Appl. Phys. **88**, 5463 (2001).
[14] Z. Qiu, N. Markarian, B. Khusid, and A. Acrivos, J. Appl. Phys. **92**, 2829 (2002).
[15] N. Markarian, M. Yeksel, B. Khusid, and A. Acrivos, Appl. Phys. Lett. **82**, 4839 (2003).
[16] D. Bennett, B. Khusid, C. D. James, P. Galambos, M. Okandan, D. Jacqmin, and A. Acrivos, Appl. Phys. Lett. **83**, 4866 (2003).
[17] W. B. Russel, D. A. Saville, and W. R. Schowalter, Colloidal Dispersions (Cambridge University Press, Cambridge, England, 1989).
[18] S. S. Dukhin and V. N. Shilov, *Dielectric Phenomena and the Double Layer in Disperse Systems and Polyelectrolytes* (Wiley, New York, 1974).
[19] B. Khusid and A. Acrivos, Phys. Rev. E **52**, 1669 (1995).
[20] B. Khusid and A. Acrivos, Phys. Rev. E **60**, 3015 (1999).
[21] B. Khusid and A. Acrivos, Phys. Rev. E **54**, 5428 (1996).
[22] L. D. Landau, E. M. Lifshitz, and L. P. Pitaevski, *Electrodynamics of Continuous Media* (Pergamon, Oxford, 1984).
[23] F. N. H. Robinson, *Macroscopic Electromagnetism* (Pergamon, Oxford, 1973).
[24] M. Ungarish, *Hydrodynamics of Suspensions* (Springer-Verlag, Berlin, 1993).